MICROSTRUCTURAL STABILITY AND OXIDATION RESISTANCE OF 9-12 CHROMIUM STEELS AT ELEVATED TEMPERATURES

O.N. Dogan[1], D.E. Alman[1], P.D. Jablonski[1], J.A. Hawk[2]
[1]National Energy Technology Laboratory, U.S. Dept. of Energy, Albany, Oregon 97321
[2]GE-Energy, Schenectady, New York

ABSTRACT

Various martensitic 9-12 Cr steels are utilized currently in fossil fuel powered energy plants for their good elevated temperature properties such as creep strength, steam side oxidation resistance, fire side corrosion resistance, and thermal fatigue resistance. Need for further improvements on the properties of 9-12 Cr steels for higher temperature (>600^{o}C) use is driven by the environmental concerns (i.e., improve efficiency to reduce emissions and fossil fuel consumption). In this paper, we will discuss the results of the research done to explore new subsitutional solute solution and precipitate hardening mechanisms for improved strength of 9-12 Cr martensitic steels. Stability of the phases present in the steels will be evaluated for various temperature and time exposures. A comparison of microstructural properties of the experimental steels and commercial steels will also be presented.

The influence of a Ce surface treatment on oxidation behavior of a commercial (P91) and several experimental steels containing 9 to 12 weight percent Cr was examined at 650ºC in flowing dry and moist air. The oxidation behavior of all the alloys without the Ce modification was significantly degraded by the presence of moisture in the air during testing. For instance the weight gain for P91 was two orders of magnitude greater in moist air than in dry air. This was accompanied by a change in oxide scale from the formation of Cr-based scales in dry air to the formation of Fe-based scales in moist air. The Ce surface treatment was very effective in improving the oxidation resistance of the experimental steels in both moist and dry air. For instance, after exposure to moist air at 650ºC for 2000 hours, an experimental alloy with the cerium surface modification had a weight gain three orders of magnitude lower than the alloy without the Ce modification and two orders of magnitude lower than P91. The Ce surface treatment suppressed the formation of Fe-based scales and promoted the formation of more protective Cr-based scales. However, the Ce surface treatment was not effective in improving the resistance of P91. The results are discussed in terms of synergistic effects of constituent alloying elements.

INTRODUCTION

Various martensitic 9-12 Cr steels are utilized currently in fossil fuel powered energy plants for their good elevated temperature properties such as creep strength, steam side oxidation resistance, fire side corrosion resistance, and thermal fatigue resistance. Need for further improvements on the properties of 9-12 Cr steels for higher temperature use is

driven by the environmental concerns (i.e., improve efficiency to reduce emissions and fossil fuel consumption) [1-4]. Use of ultrasupercritical (USC) steam conditions in the new power plants is expected to achieve the increased efficiency. Several martensitic steels with 9-12 wt. pct. Cr content are being developed for the USC conditions in Japan and Europe [5-6].

A series of recently developed 9-12 Cr steel compositions has been tested for elevated temperature applications at the National Energy Technology Laboratory. These steels are precipitation strengthened with TiC and Cu-rich particles and solid solution strengthened with Co, Cu, Ni and Mo additions. The aim of the present investigation was to assess the mechanical and oxidation behavior of the experimental 9-12 Cr alloys and to investigate a strategy whereby rare earth elements (i.e., Ce, La, Y) are used to improve oxidation resistance.

EXPERIMENTAL PROCEDURE

Steels used in this investigation were melted in a vacuum induction furnace using precursor elemental charge materials. These experimental alloys were designated as HR52, HR53, and HR 54. A commercial steel (P91) was also tested as a comparison material. Chemical composition of these steels is listed in Table 1. The molten alloys were poured and solidified in a graphite mold with 2 in diameter and 6 in height. After removing the hot tops and surface layer, the ingots were hot forged and rolled to 0.5 in thick plates. Test specimens were cut from the plates.

Table 1. Nominal and actual (in *italic*) compositions in weight percent. Balance is Fe.

Alloy	Cr	C	Cu	Co	Ni	Mo	Ti	Mn	Si	Nb	V
HR52	9 *9.06*	0.1 *0.08*	3 *2.94*	3 *3.03*	1 *1.19*	0.7 *0.69*	0.5 *0.50*	-	-	-	-
HR53	10.5 *10.54*	0.1 *0.08*	3 *2.99*	4 *4.04*	1 *1.19*	0.7 *0.70*	0.5 *0.54*	-	-	-	-
HR54	12 *11.80*	0.1 *0.08*	3 *2.97*	4 *3.96*	1 *1.19*	0.7 *0.69*	0.5 *0.51*	-	-	-	-
P91	9 *8.26*	0.1	- *0.12*	-	- *0.32*	1 *0.92*	-	0.45 *0.51*	0.4 *0.34*	0.08 *0.08*	0.2 *0.23*

Ti was determined by inductively coupled plasma (ICP), C was determined by combustion (Leco), and all other elements were determined by x-ray fluorescence (XRF).

The specimens were heat treated at 750ºC for 0, 1, 10, 100, and 1000 hours. They were designated as T1, T2, T3, T4, and T5, respectively. Microstructure was characterized using optical and scanning electron microscopy (SEM). X-ray diffraction (XRD) was also employed for phase determination. Quantitative analysis of precipitates was performed using an image analyzer. A thermodynamic simulation software (ThermoCalc®) was used to study the equilibrium phases in these alloys. The steel database (TCFE3) was used in the calculations.

Hardness testing was performed at room and elevated temperatures. A Rockwell hardness machine was employed to measure the room temperature hardness of the as cast (in C

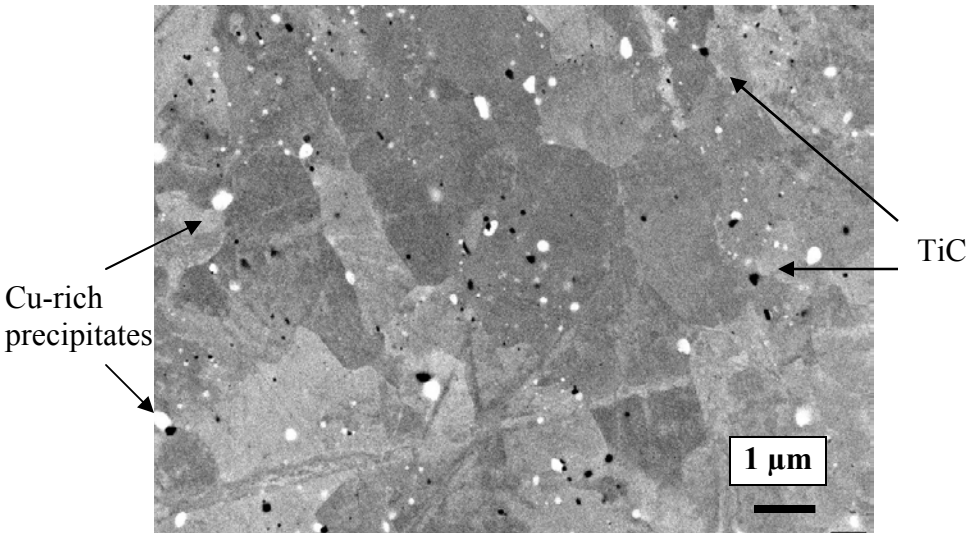

Figure 1. Backscattered electron image of HR54 after 100 hours at 750ºC showing TiC and Cu-rich precipitates.

scale) and as heat treated (in B scale) specimens. A Vickers indenter under 1 kg load was used to measure hardness at elevated temperatures up to 700ºC. The hot hardness testing was performed in vacuum. Tensile testing of the heat treated specimens was performed at room temperature using a screw driven machine at 0.5 mm/min loading rate. Fracture surfaces were examined using SEM.

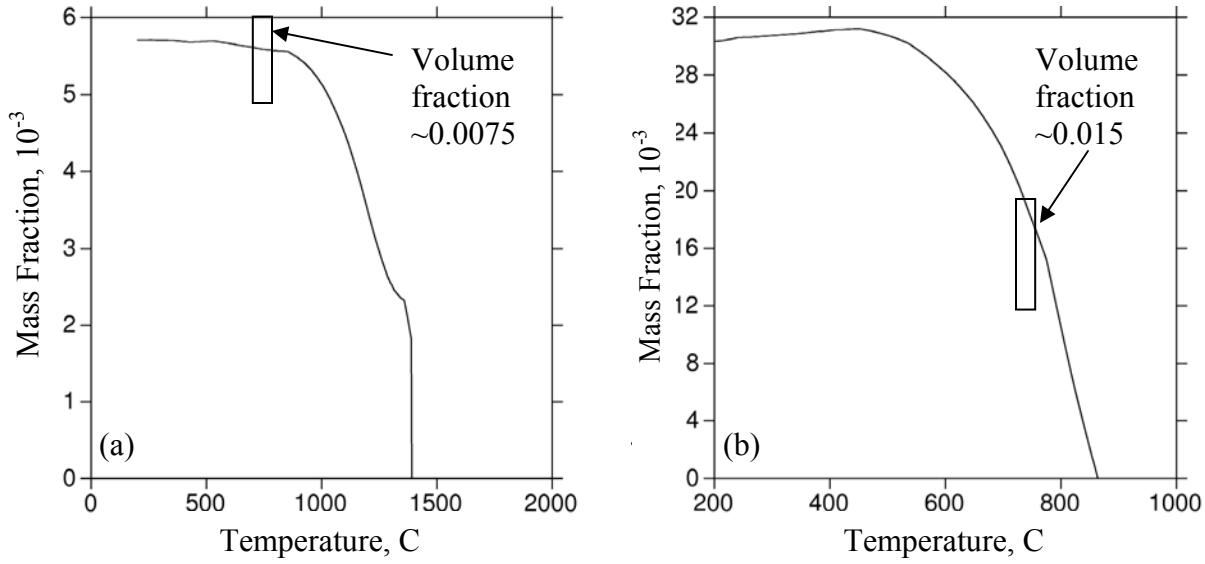

Figure 2. Thermodynamic calculations and experimental data (rectangles) for mass fraction of precipitates in HR53 after 100 hours at 750ºC (a) TiC and (b) Cu-rich precipitates.

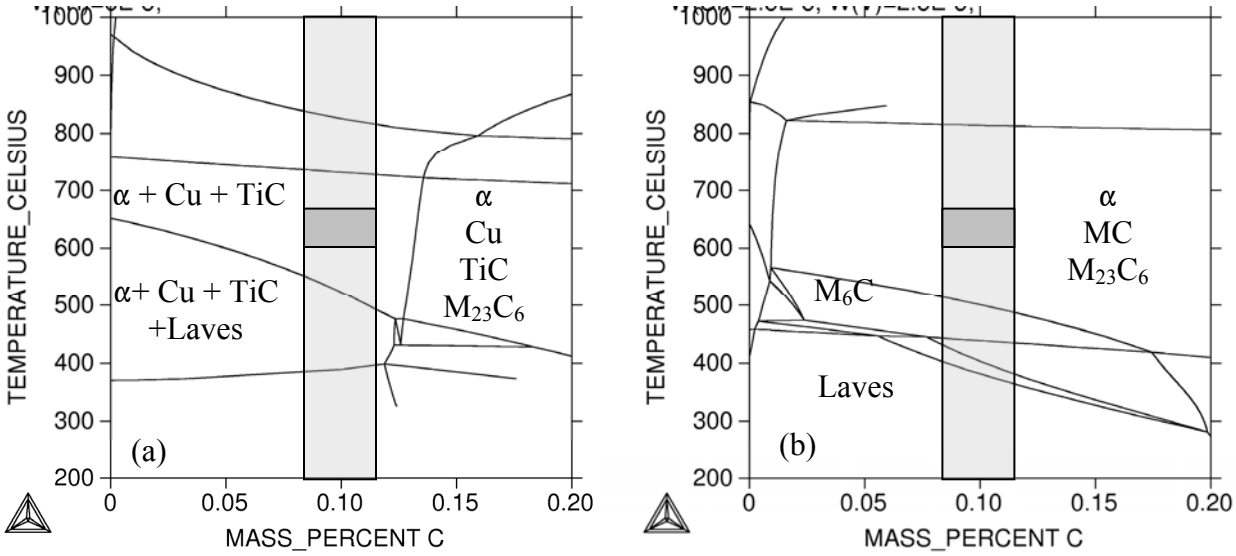

Figure 3. Carbon isopleths for HR52 (a) and P91 (b) as calculated using ThermoCalc®. Carbon content of these steels is highlighted with light gray and intended temperature range of application is marked with dark gray.

Cyclic oxidation behavior of the experimental alloys was studied in dry air and moist air (air with 3% H_2O) at 650ºC. The oxidation coupons (19mm x 19mm x 5mm) were cut from the rolled plates and ground for a 600 grit surface finish. The coupons were cleaned in alcohol ultrasonically and weighed. They were placed in a quartz rack and inserted in a tube furnace at 650 ºC. Dry or moist air was flowed over the coupons during the experiments.

In addition, effect of cerium infusion [7] on the surface of oxidation coupons was investigated. This method consists of applying a slurry containing the RE element to the surface of a coupon via dip coating, painting or spraying. The slurry is then reacted with the alloy at high temperature to infuse Ce into the surface. After treating, excess slurry is removed by simply rinsing the treated sample in water. The treated coupons were tested and analyzed along with the untreated samples using the procedures described above. The Ce surface infused samples are identified as HR52+Ce, HR53+Ce and HR54+Ce, respectively. During all of the tests (with or without Ce infusion), the specimens were taken out of the furnace and weighed periodically. Mass change of the specimens was recorded as a function of exposure time. Oxidation scales were characterized using SEM and XRD.

RESULTS AND DISCUSSION

Microstructure

Matrix of HR alloys was predominantly martensitic as determined using optical microscopy and XRD. A small amount of delta ferrite was present in all compositions.

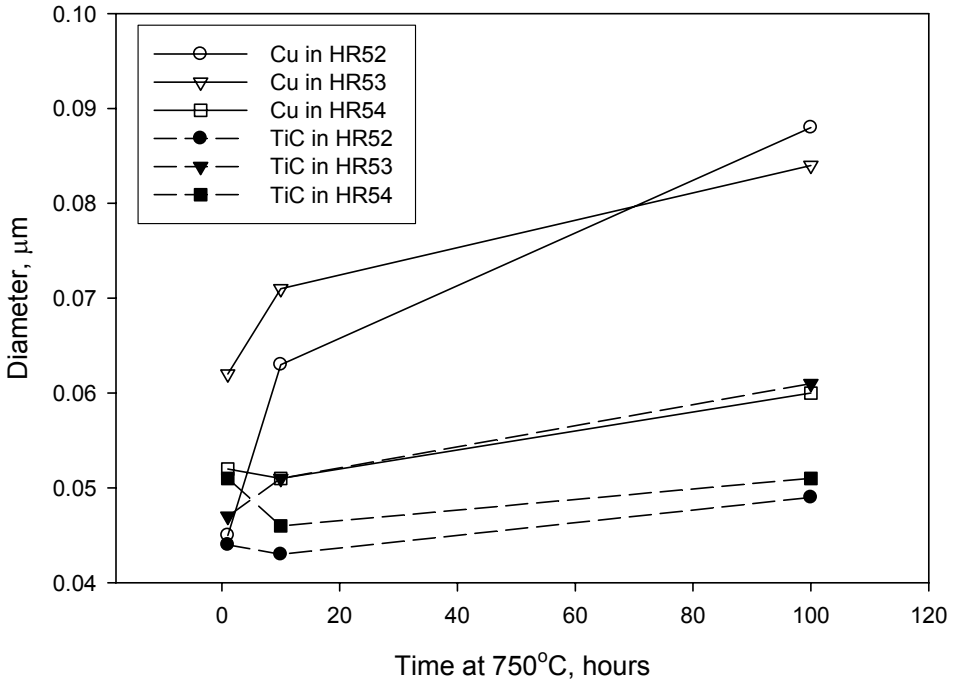

Figure 4. Coarsening behavior of TiC and Cu-rich precipitates in the HR steels at 750ºC.

With increasing Cr content from HR52 to HR54, the amount of delta ferrite increased. This was the case in both the as cast and as rolled and heat treated specimens. After the hot rolling, a dispersion of precipitates was observed in the HR alloys. Two different types of precipitates were identified. They were copper rich precipitates with a higher volume fraction and a larger average size and titanium carbide precipitates with finer size distribution. A back scattered electron image in Figure 1 demonstrates these precipitates in HR54-T4 after 100 hours at 750ºC. Mass fraction of Cu and TiC precipitates in HR53 was measured using an image analyzer and compared to the results from the equilibrium calculations in Figure 2. The experimental observations agreed with the calculations reasonably well. Thermodynamic prediction of phases in the HR52 and the commercial P91 alloys is shown in the form of a carbon isopleth in Figure 3. Both steels contain about 0.1 mass percent C. At this carbon content, the equilibrium phases in HR52 is bcc Fe, Cu-rich precipitates, and TiC precipitates at the application temperature of 600ºC to 650ºC. The phase field of $M_{23}C_6$ and Laves phase is avoided in HR alloys. P91 is predicted to have $M_{23}C_6$ unless the carbon content is below 0.01 mass percent at the same temperature range. The other equilibrium phases in P91 are the bcc Fe and NbC.

Figure 4 shows the increase in size of the precipitates with time at 750ºC. Generally, the TiC precipitates are smaller (40-60 nm) and they coarsen slower. On the other hand, the Cu-rich precipitates tend to be larger (50-80 nm) and their coarsening kinetics is faster.

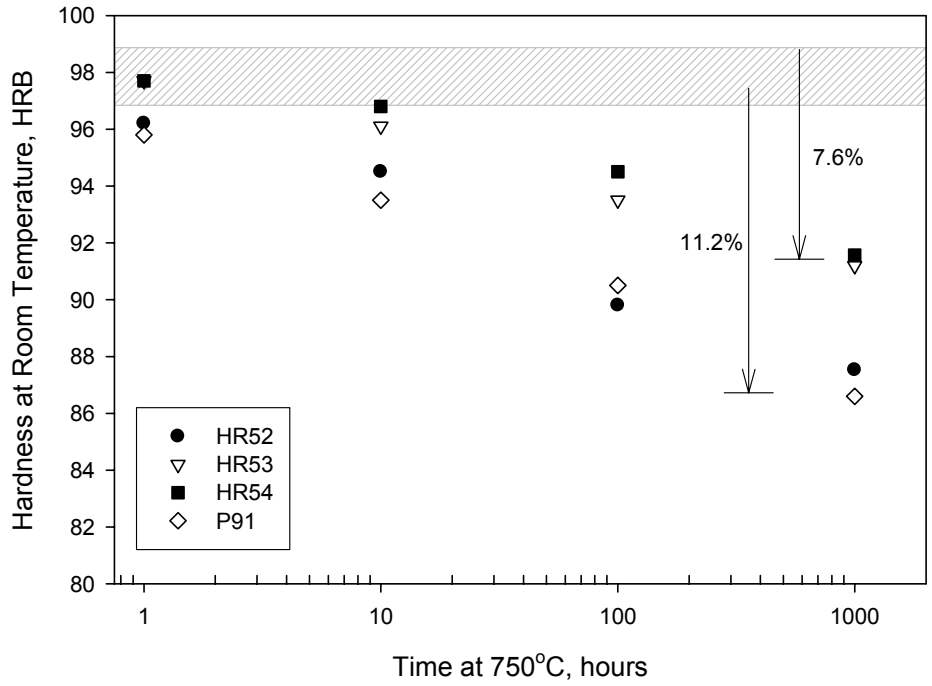

Figure 5. Room temperature hardness (Rockwell B) of the steels after the heat treatment at 750ºC. The shaded area shows the hardness range before the heat treatment.

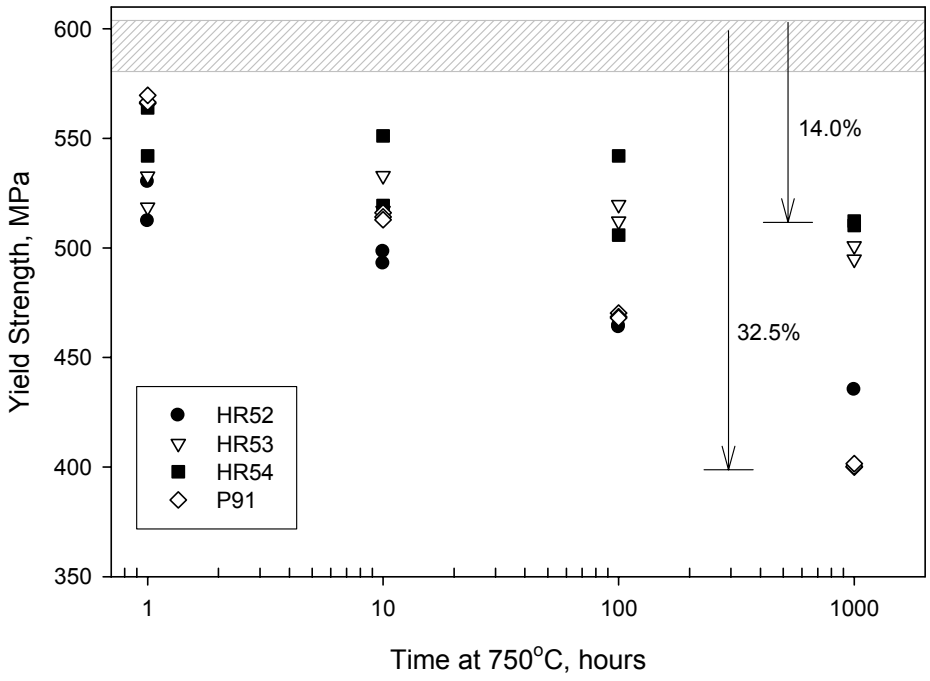

Figure 6. Yield strength of the steels at room temperature after the heat treatment at 750ºC. The shaded area shows the yield strength range before the heat treatment.

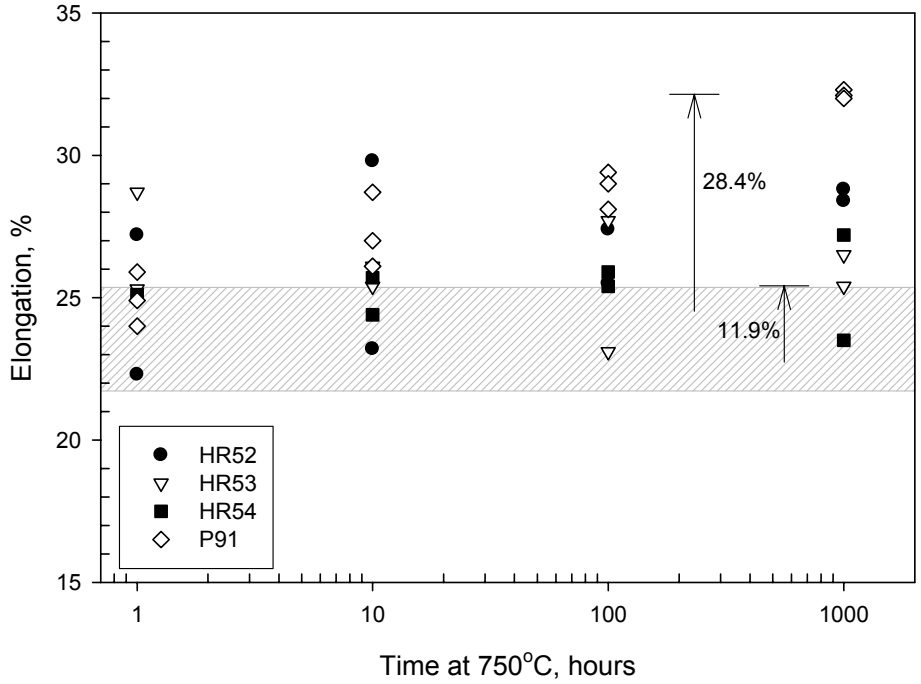

Figure 7. Tensile elongation of the steels at room temperature after the heat treatment at 750ºC. The shaded area shows the elongation range before the heat treatment.

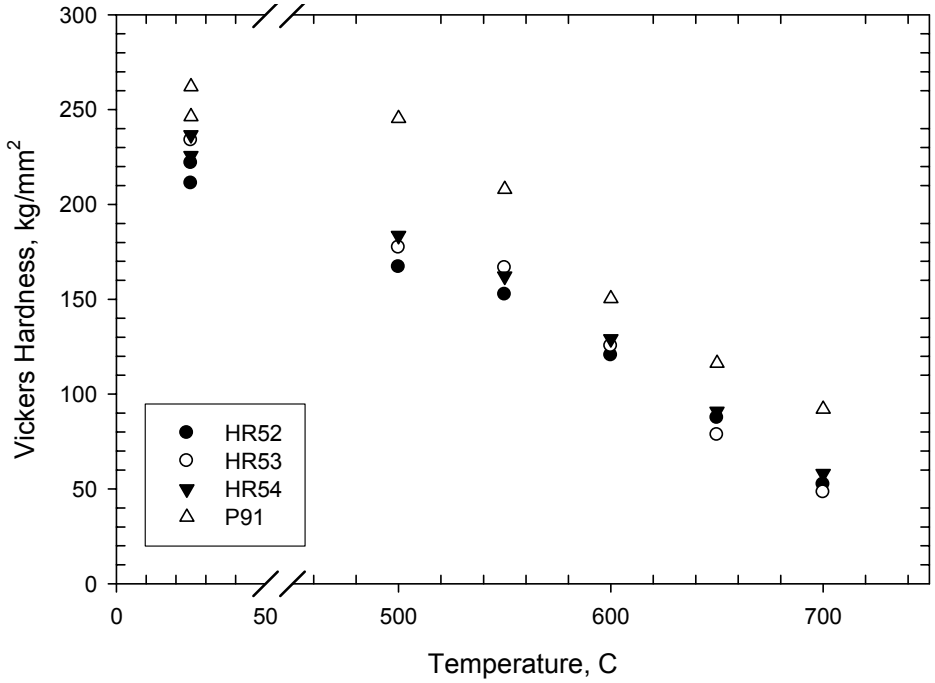

Figure 8. Hardness of the HR and P91 steels at elevated temperatures.

Mechanical Properties

Room temperature hardness of the specimens was determined after they were held at 750ºC up to 1000 hours. Figure 5 shows the change in hardness at room temperature with exposure time at 750ºC. For all steels investigated, hardness decreased with increasing exposure time. The rate of decrease was faster for the lower Cr alloys (P91 and HR52). The hardness of P91 decreased 11.2% from its as rolled hardness whereas the hardness of HR53 and HR54 decreased 7.6% after 1000 hours at 750ºC.

Similarly, yield strength of the P91 decreased after 1000 hour exposure more than the experimental alloys (Figure 6). The decrease in the yield stress of P91 was 32.5% from its as-received state (from about 600MPa to 400MPa). The lowest decrease in yield strength was observed in HR54 (14.0%). Corresponding increase in elongation for the HR alloys and P91 steel is shown in Figure 7.

Hardness of the HR steels and the P91 steel was measured at elevated temperatures. The results are shown in Figure 8. Up to 500ºC, P91 steel preserved most of its room temperature hardness. However, it experienced a dramatic drop in hardness above 500ºC. On the other hand, the decrease in hardness with temperature was more gradual in the HR alloys. At the application temperature range of 600ºC to 650ºC, the P91 alloy had a somewhat higher hardness than the HR alloys.

Fracture surfaces of the tensile specimens were examined using SEM. Fracture surfaces were characterized by a combination of large and small dimples, cleavage aspects, and

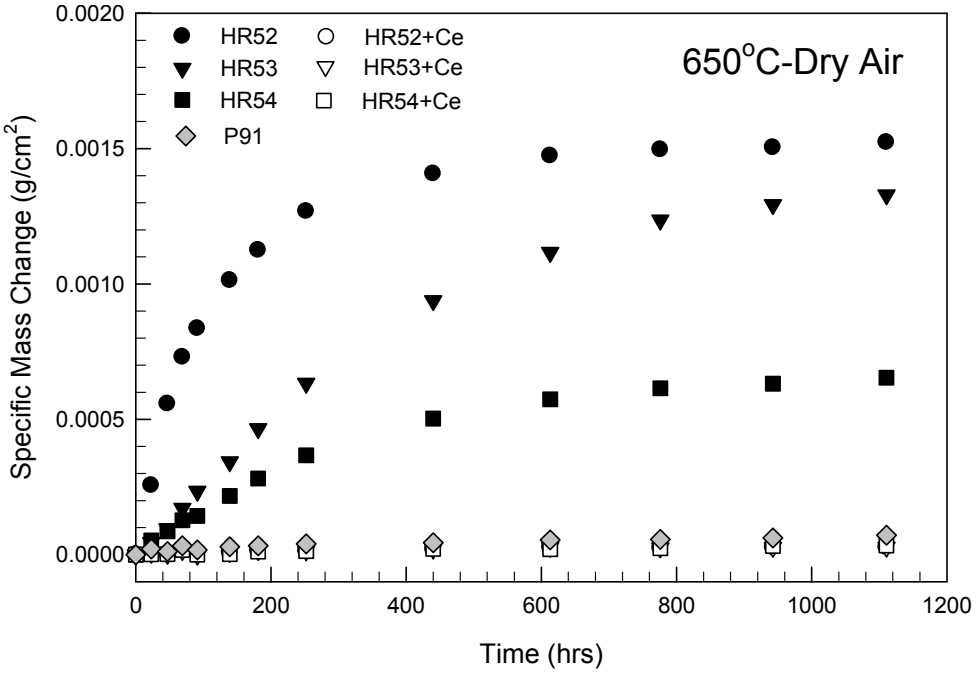

Figure 9. Oxidation kinetics of the steels with and without Ce infusion at 650ºC in dry air.

fissures in all of the experimental alloys and P91. Macroscopic cleavage aspects were no longer present in the HR alloys after 1000 h exposure at 750ºC. Small dimples contained nanometer size particles whereas the large dimples contained particles larger than 1 μm in size or composed of an agglomeration of smaller particles. The fissures were composed of a line of large particles arranged along a grain boundary.

Table 2. Oxide phases as determined by x-ray diffraction.

Alloy	Condition	Oxide
HR52	Dry air at 650ºC	Fe_2O_3, $Fe_{1.2}Cr_{0.8}O_3$, $Cr_{1.3}Fe_{0.7}O_3$, $FeCr_2O_4$
HR53	Dry air at 650ºC	Cr_2O_3, $Cr_{1.3}Fe_{0.7}O_3$, $FeCr_2O_4$, Fe_2O_3, Fe_3O_4
HR54	Dry air at 650ºC	Cr_2O_3, $Fe_{1.2}Cr_{0.8}O_3$, $Cr_{1.3}Fe_{0.7}O_3$, Fe_3O_4
P91	Dry air at 650ºC	$Mn_{1.5}Cr_{1.5}O_4$, Fe_2O_3, $FeMnO_3$
HR52 + Ce	Dry air at 650ºC	Cr_2O_3, $Cr_{1.3}Fe_{0.7}O_3$, CeO_2
HR53 + Ce	Dry air at 650ºC	Cr_2O_3, $Cr_{1.3}Fe_{0.7}O_3$, CeO_2
HR54 + Ce	Dry air at 650ºC	Cr_2O_3, CeO_2
HR52	Moist air at 650ºC	Fe_2O_3, $FeCr_2O_4$
P91	Moist air at 650ºC	Fe_2O_3, $FeCr_2O_4$
HR52 + Ce	Moist air at 650ºC	Cr_2O_3, $Cr_{1.3}Fe_{0.7}O_3$, CeO_2
P91 + Ce	Moist air at 650ºC	Fe_2O_3, CeO_2

Oxidation

Figure 9 shows specific mass change of the alloys during the cyclic oxidation at 650ºC in dry air. All alloys tested followed a parabolic oxidation rate. Oxidation resistance of the experimental HR alloys increased with increasing Cr content. Even with the highest Cr content of 12 mass %, these steels oxidized at a faster rate than the P91 steel. This is attributed to the lack of Mn and Si in the HR alloys which contribute to the oxidation resistance of these steels by modifying growth characteristics of the oxidation scale.

XRD analysis done on the steels after the oxidation tests revealed different types of oxides in the scales as summarized in Table 2. Two types of $(Fe,Cr)_2O_3$ oxides were found. One was an Fe-rich oxide while the other was a Cr-rich oxide. Fe_2O_3 and $FeCr_2O_4$ were detected on the surfaces of both the 9 and 10.5 wt. pct. Cr alloys (HR 52 and HR 53). While, Cr_2O_3 and Fe_3O_4 were detected on the 10.5 and 12 wt. pct. Cr alloys (HR 53 and HR 54). The analysis of the oxidation scales on the HR alloys was reported in more detail elsewhere [8].

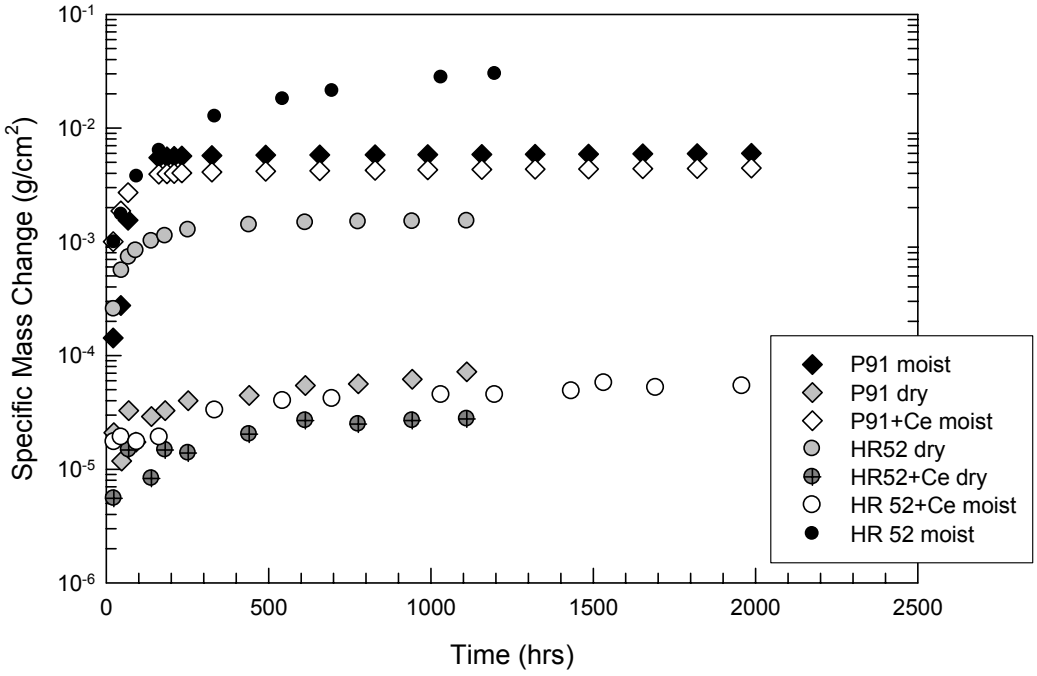

Figure 10. Oxidation kinetics of HR52 and P91 with and without Ce infusion at 650ºC in dry and moist air.

Effect of cerium infusion on the surface of the HR alloys and P91 during the cyclic oxidation tests at 650ºC in dry air is also shown in Figure 9. The performance of all HR alloys with Ce incorporated into the surface was quite remarkable. The mass gains of the treated alloys were all approximately 0.03 mg/cm^2, more than an order of magnitude lower then the alloys without the Ce surface infusion. Furthermore, the treated alloys exhibited essentially equivalent mass gain results, regardless of the initial Cr level. XRD results on the Ce infused alloys are also summarized in Table 2. Cr_2O_3 and CeO_2 were detected on the surface of all the alloys given the Ce surface infusion treatment. Cr-rich, $(Cr,Fe)_2O_3$ also formed on the surface treated samples of the lower Cr alloys (HR 52+Ce and HR 53+Ce).

Influence of moisture on the steady state oxidation kinetics is shown in Figure 10 for HR52 and P91. The cyclic oxidation tests in air containing 3 vol. pct. H_2O at 650ºC were performed up to 2000 hours. The specific mass gain in the moist condition was more than an order of magnitude higher than in dry air for both HR52 and P91. The Ce infusion on the surface of HR52 lowered the oxidation kinetics drastically under the moist condition whereas the same treatment under the same test conditions did not make any significant difference in the oxidation kinetics of P91. The significant improvement in the case of HR52 is attributed to the formation of Cr_2O_3 as the prominent oxide in the scale instead of Fe_2O_3. On the other hand, the XRD results showed that the prominent oxide (Fe_2O_3) did not change in the case of P91.

SUMMARY

Thermodynamic calculations predict equilibrium phases as bcc-Fe, TiC, and Cu-rich phase at the possible application temperature range of 600ºC-650ºC for the experimental 9-12Cr steels. In both the as cast and rolled conditions, these steels are primarily martensitic with some delta ferrite. As the Cr level increases from 9 to 12 wt%, the amount of delta ferrite in the matrix increases.

Both TiC and Cu-rich precipitates provide strengthening. After up to 100h treatment at 750C, the TiC precipitates do not coarsen significantly. On the other hand, the Cu-rich precipitates coarsen at a faster rate.

P91 shows larger decreases in hardness and yield stress compared to HR53 and HR54, and similar behavior to HR52 after the exposure at 750ºC up to 1000 hours. Increasing Cr levels in HR53 and HR54, and the incorporation of Cu and Co in the HR series of alloys, lead to a lower rate of mechanical property deterioration.

The oxidation resistance of the alloys at 650ºC in dry air increased with increasing Cr content, resulting in lower mass gain during oxidation. Reduction in oxidation resistance with decreasing Cr content was attributed to the formation of non-protective Fe-oxide nodules on the surface of the untreated alloys. The concentration of these nodules decreased as the Cr level in the alloy increased.

Cerium infused into the surface of the alloys significantly increased oxidation resistance, as the mass gain decreased by more than an order of magnitude compared to the alloys without Ce infusion. The specific mass gain in the moist condition was more than an order of magnitude higher than in dry air for both HR52 and P91.

ACKNOWLEDGEMENTS

The authors would like to thank P. Danielson, K. Collins, R. Chinn, N. Duttlinger, and E. Argetsinger of the NETL-Albany for assistance with metallography and image analysis, SEM, x-ray diffraction, mechanical testing, and alloy preparation, respectively.

REFERENCES

1. R. Viswanathan and W. Bakker, JMEPEG (2001), 10, 81-95.
2. P.J. Ennis and A. Czyrska-Filemonowicz, OMMI (2002), 1 (1), 1-28.
3. R. Viswanathan, J.F Henry, J. Tanzosh, G. Stanko, J. Shingledecker, and B. Vitalis, Proceedings from the Fourth International Conference on Advances in Materials Technology for Fossil Power Plants, October 25-28, 2004, Hilton Head Island, South Carolina, ASM International, Materials Park, Ohio (2005), 3-19.
4. T. Fujita, Advanced Materials & Processes (2000), 6, 55-58.
5. B. Scarlin, T-U. Kern, M. Staubli, Proceedings from the Fourth International Conference on Advances in Materials Technology for Fossil Power Plants,

October 25-28, 2004, Hilton Head Island, South Carolina, ASM International, Materials Park, Ohio (2005), 80-99.
6. F. Abe, Proceedings from the Fourth International Conference on Advances in Materials Technology for Fossil Power Plants, October 25-28, 2004, Hilton Head Island, South Carolina, ASM International, Materials Park, Ohio (2005), 202-216.
7. P.D Jablonski, D.E. Alman, S.C. Kung, Ceram. Engr. Sci. Proc., vol.26, American Ceramic Society, Westerville, Ohio, (2005), p.193.
8. D.E. Alman, W.K. Collins, O.N. Dogan, J.A. Hawk, P.D. Jablonski, submitted to Oxidation (2005).